EPJ manuscript No.
(will be inserted by the editor)

Bursting oscillations and bifurcation mechanism in a fully integrated piecewise-smooth chaotic system

Minglin Ma[1,a], Yingjun Fang, Zhijun Li, Yichuang Sun[2], and Mengjiao Wang

[1] College of Automation and Electronic Information, Xiangtan University, Xiangtan 411105, P.R. China,
[2] School of Engineering and Technology, University of Hertfordshire, Hatfield, AL10 9AB, U.K.

Abstract. This paper aims to show and investigate bursting oscillator and bifurcation phenomena in a piecewise-smooth memristor-based Shimizu–Morioka (SM) system. To make the circuit low power consumption and portable in practice, it is fully integrated. In the paper, a periodic excitation and different piecewise functions are introduced into the system which leads to two types of piecewise-smooth systems with a single slow variable. As the slow variable changes periodically in different scopes, we discover intricate bursting oscillation phenomena, namely, asymmetric Fold/Fold bursting, damped oscillation-sliding, asymmetric Fold/Fold-delayed supHopf/supHopf bursting, compressed oscillation phenomenon within the limit cycle, random bursting, double loop oscillations and so on. In the course of the study, it is found that the properties of the nominal equilibrium orbits, limit cycles, and the non-smooth boundary contribute to the bursting. Finally, a fully integrated circuit is designed and the accuracy of the study is verified by some circuit simulation results.

Key words. Bursting, Bifurcation, Piecewise, Memristor, Integration

1 Introduction

Piecewise-smooth systems have attracted wide attention due to many special behaviors such as non-conventional bifurcations. For example, Zhang et al. based on the chaotic geomagnetic field model, introduced a non-smooth factor to explore complex dynamical behaviors [1]. Similarly, reports based on the typical Chua's system [2,3] and a piecewise mechanical system [4] also exhibit different forms of bursting oscillations. Lately, some new research advances have been found in this area which contribute to the theoretical and practical basis [5-8]. Such dynamical systems including the piecewise-smooth Shimizu–Morioka system in this paper involve different timescales especially two timescales [9-11]. Generally, when all state variables are almost at rest, the system is in a quiescent state (QS) stage. Conversely, the two

[a] e-mail: minglin_ma@xtu.edu.cn

timescales may give rise to spiking state (SP) when all state variables show themselves as large-amplitude oscillations [12-14]. If the state variables transform between QS and SP, bursting phenomena can be observed [15,16]. Using the slow-fast analysis, the vector fields can be divided into a slow subsystem and a fast subsystem which is easy to analyze the bursting mechanism [17-19].

The memristor is a natural nonlinear element firstly hypothesized by Chua [20]. The memristor-based circuits and systems have been widely researched recently because of the initial sensitivity and high randomicity [21-28]. In the field of bursting oscillations, several new phenomena are found in the memristor-based systems. Typically, N. Henry Alombah's Multiscroll memristive chaotic circuit displays bursting oscillations called fold-Hopf type [29]. What is more, Wang's simple memristor-capacitor-based chaotic circuit [30], Wen's memristor-based Shimizu-Morioka system [31], Bao's third-order autonomous memristor-based system [32] and Wu's memristive Wien-bridge oscillator [33] also manifest complex bursting oscillations. However, to the best of our knowledge, research on the bursting oscillations and bifurcation mechanism in a piecewise-smooth memristor-based SM system has not been studied.

It is easy to see that the development direction of modern electronic devices is miniaturization and integration such as integrated operational amplifiers, power amplifiers, etc. Recently, some of the existing chaos generators are designed with integration technology [34,35]. Its advantages are lower supply voltage, lower power dissipation, and smaller chip area. We can also introduce this technology to our chaos generator.

Summing up the above, a piecewise-smooth memristor-based SM system is created to explore the new bursting phenomena. In Section 2, we explain the system mathematically. Bifurcation and stability analysis is given in Section 3. Section 4 shows intricate bursting oscillation phenomena and the bifurcation mechanism. We build a fully integrated circuit and relevant circuit simulation results are obtained in Section 5. The final section concludes the paper.

2 Mathematical model

A memristor, an AC excitation w, and piecewise functions are introduced into the SM system to establish the following piecewise-smooth memristor-based SM system model. According to the number of segmentations, two systems are given below.

2.1 Type-I

$$\begin{aligned}\dot{x} &= y\\ \dot{y} &= [x+g(x)] - ay - [x+g(x)]z + kM(x)y + w\\ \dot{z} &= -bz + [x+g(x)]^2\end{aligned} \tag{1}$$

Thereinto, $w = Asin(\omega t)$, indicates that the slow variable is a sinusoidal signal with amplitude A and frequency ω. State variables are defined as x, y, z, and a, b, k are system parameters. As for the memristor, its equation is

$$M(x) = -n + [x+g(x)]^2$$

As mentioned above, the piecewise function is $g(x) = [sgn(x-1)-1]/2$. On the basis of system (1), the non-smooth boundary $\Sigma : \{(x,y)|x=1\}$ divides the system into two smooth sub-regions, denoted as $D_+ : \{(x,y)|x>1\}$ and $D_- : \{(x,y)|x<1\}$, while D_+, D_- correspond to different subsystems.

2.2 Type-II

$$\begin{aligned}
&\dot{x} = y \\
&\dot{y} = [x - f(x)] - ay - [x - f(x)]z + kM(x)y + w \\
&\dot{z} = -bz + [x - f(x)]^2 \\
&M(x) = -n + [x - f(x)]^2
\end{aligned} \tag{2}$$

Compared with system (1), the piecewise function is changed. In system (2), the piecewise function is $f(x) = [sgn(x-2) + sgn(x+2)]/2$. The whole state phase plane is divided into three smooth sub-regions, indicated as $D_\alpha : \{(x,y)|x > 2\}$, $D_\beta : \{(x,y)| - 2 < x < 2\}$, and $D_\gamma : \{(x,y)|x < -2\}$ due to the non-smooth boundary $\Sigma_1 : \{(x,y)|x = 2\}$ and $\Sigma_2 : \{(x,y)|x = -2\}$. Likewise, D_α, D_β, and D_γ correspond to respective subsystems.

Above all, on the one hand, setting $0 < \omega \ll 1$, thus the external excitation w changes very slowly. At the same time, the natural frequency of the system $\Omega \gg \omega$, so the system exhibits the coupling effect between different scales in the frequency domain. Between two subsystems, the fast subsystem will determine the manifestation of QS and SP, while the slow subsystem will regulate the motion trajectory of the system, resulting in bursting oscillations and other special dynamic behaviors. On the other hand, due to the effect of the piecewise function, the system can produce complex non-smooth phenomena. Therefore, under the contribution of these two factors, many new bursting phenomena may occur.

3 Bifurcation and stability analysis

3.1 Type-I piecewise-smooth memristor-based SM system

Comparing system (1) with the traditional SM system based on memristor [31], we can find the only difference is that there is a segmentation control $g(x) = [sgn(x-1)-1]/2$ together with the x state variable. As a result, the number of the equilibrium curve changes from one to two, which means two subsystems should be considered.

According to equations (1), $g(x)$ changes with the value of x. When taking $x < 1$ into account, we get $g(x) = -1$, and equations (1) become as follows

$$\begin{aligned}
&\dot{x} = y \\
&\dot{y} = (x-1) - ay - (x-1)z + k[(x-1)^2 - n]y + w \\
&\dot{z} = -bz + (x-1)^2
\end{aligned} \tag{3}$$

In this region, the equilibrium point of the subsystem D_- can be expressed as $E0(x,y,z) = (x_0, 0, \frac{(x_0-1)^2}{b})$, while x_0 always satisfies the following equation, namely

$$(x_0-1)^3 - b(x_0-1) - bw = 0 \tag{4}$$

and the stability matrix of this equation is

$$\mathbf{J} = \begin{pmatrix} 0, & 1, & 0 \\ 1 - \dfrac{(x_0-1)^2}{b}, & -a + k[(x_0-1)^2 - n], & -(x_0-1) \\ 2(x_0-1), & 0, & -b \end{pmatrix} \tag{5}$$

According to the matrix, the characteristic equation is written as

$$\lambda^3 + \lambda^2\{a + b - k[(x_0 - 1)^2 - n]\} + \lambda\{ab - bk[(x_0 - 1)^2 - n] - 1 + \frac{(x_0 - 1)^2}{b}\}$$
$$+ 3(x_0 - 1)^2 - b = 0 \tag{6}$$

Based on the Routh-Hurwitz criterion, the equilibrium point $E0$ is stable when

$$\begin{aligned} &3(x_0 - 1)^2 - b > 0 \\ &a + b - k[(x_0 - 1)^2 - n] > 0 \\ &\{a + b - k[(x_0 - 1)^2 - n]\} \cdot \{ab - bk[(x_0 - 1)^2 - n] - 1 + \frac{(x_0 - 1)^2}{b}\} \\ &- [3(x_0 - 1)^2 - b] > 0 \end{aligned} \tag{7}$$

The stability of the equilibrium will be influenced when w alters, leading to two different types of bifurcation. However, due to the limitation of x, some bifurcations are not real.

When $3(x_0 - 1)^2 - b = 0$, the corresponding characteristic roots pass through the zero value, and the equilibrium point becomes unstable. It can be seen from equation (4) that the equilibrium curve shows a typical S-shape, so the system may manifest Fold bifurcation.

As we consider, Hopf bifurcation will also exist when x_0 meets with the equation

$$\{a + b - k[(x_0 - 1)^2 - n]\} \cdot \{ab - bk[(x_0 - 1)^2 - n] - 1 + \frac{(x_0 - 1)^2}{b}\}$$
$$- [3(x_0 - 1)^2 - b] = 0 \tag{8}$$

At this point, it is known from the calculation that the solutions are a pair of pure imaginary roots, so periodic oscillations may occur.

Based on the analyses, if we take $a = 0.8$, $b = 0.4$, $n = 2$, and $k = 0.6$, the bifurcation set is plotted in Fig. 1(a) which shows the bifurcation situation of Ehe subsystem D_-. As we can see, there is a Fold bifurcation point FB_2^- and a Hopf bifurcation point $supH2^-$ in the equilibrium curve.

Similarly, if we consider $x > 1$, the value of $g(x)$ is 0, leading equations (1) to a different form

$$\begin{aligned} \dot{x} &= y \\ \dot{y} &= x - ay - xz + k(x^2 - n)y + w \\ \dot{z} &= -bz + x^2 \end{aligned} \tag{9}$$

Following the analyses of the subsystem D_-, we can get the bifurcation set of the subsystem D_+ in Fig. 1(b). Since the value of x is over 1, one can find there is only a Hopf bifurcation point $supH1^+$ in this subsystem.

3.2 Type-II piecewise-smooth memristor-based SM system

Since the only difference between system (2) and system (1) is the piecewise function, the equilibrium stability analysis method of the type-II system is almost identical with the type-I system. The number of the equilibrium curve is three, manifested by $x_{0\alpha}$, $x_{0\beta}$, and $x_{0\gamma}$. The Fold bifurcation and the Hopf bifurcation may also appear. The detailed analysis will not be repeated and the bifurcation sets of these three subsystems are plotted in Fig. 2.

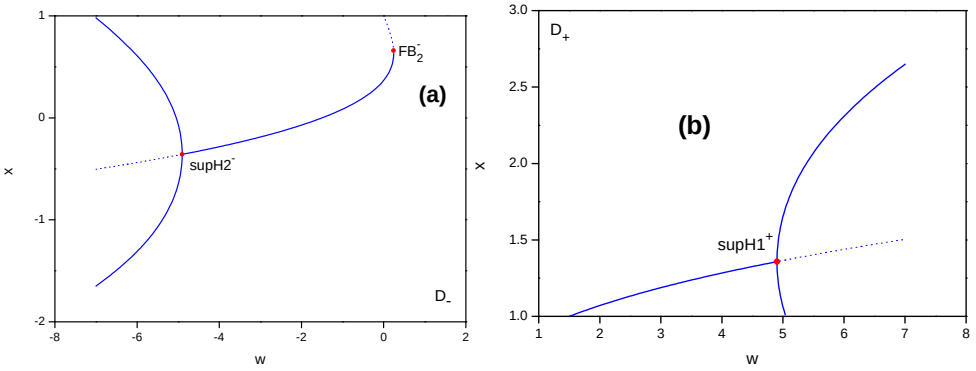

Fig. 1. The equilibrium distribution and bifurcation diagrams of the type-I system. (a) subsystem D_-, (b) subsystem D_+.

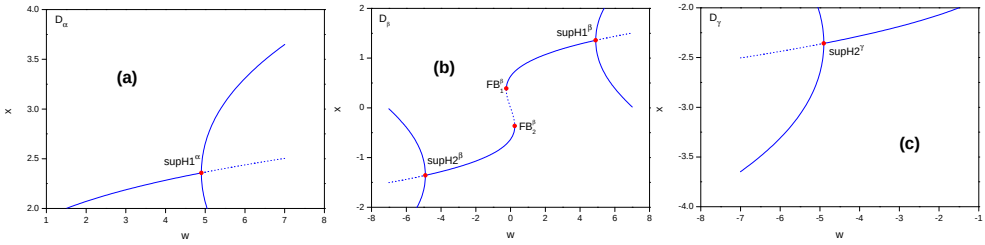

Fig. 2. The equilibrium distribution and bifurcation diagrams of the type-II system. (a) subsystem D_α, (b) subsystem D_β, (c) subsystem D_γ.

4 Bursting oscillations mechanisms

4.1 Type-I piecewise-smooth memristor-based SM system

For the convenience of discussion, based on the analyses of 3.1, we merge the subsystem D_+ and D_- (see Fig. 1) into one. The bifurcation sets of w are plotted in Fig. 3. In these two pictures, the solid lines denote stable solutions and the dotted lines denote unstable solutions. Although the red curves indicate that the solutions exist, due to the non-smooth boundary, such solutions cannot be achieved. On the contrary, the curves shown in blue are real because the solutions and the corresponding subsystem are in the same domain. One can find that the blue curves in Fig. 3(b) correspond to the curves in Fig. 1.

As can be seen from Fig. 3, the two subsystems contain four Fold bifurcation points and four Hopf bifurcation points. For the subsystem D_-, there is an intersection point M_1(0,1) between the equilibrium curve and the non-smooth boundary. The Fold bifurcation points are FB_2^-(0.24,0.63) and FB_1^-(-0.24,1.37), Hopf bifurcation points are $supH1^-$(4.90,2.36) and $supH2^-$(-4.90,-0.36) respectively. The equilibrium curve and the limit cycles are divided into 8 parts with different properties, namely, EB_1^-, EB_2^-, EB_3^-, EB_4^-, EB_5^-, EB_6^-, $LC1^-$, and $LC2^-$. Among them, EB_1^- and $LC2^-$ are stable, EB_2^- and EB_6^- are unstable, and they are all realizable; EB_4^- and $LC1^-$ are stable, EB_3^- and EB_5^- are unstable. However, due to the influence of the non-smooth boundary, they are not realizable. For the subsystem D_+, there are two intersection points with the non-smooth boundary, namely M_2(1.51,1) and M_3(5.04,1).The Fold bifurcation points are FB_2^+(0.24,-0.37) and FB_1^+(-0.24,0.37), the Hopf bifurcation points are $supH1^+$(4.90,1.36) and $supH2^+$(-4.90,-1.36), respec-

tively. The equilibrium curve and the limit cycles are divided into nine parts with different properties including EB_1^+, EB_2^+, EB_3^+, EB_4^+, EB_5^+, EB_6^+, $LC1^+$, $LC2^+$ and $LC3^+$. Thereinto, EB_4^+, $LC1^+$ are stable, EB_5^+ is unstable. Because the solutions and the corresponding subsystem are in the same domain, these curves are real. Oppositely, due to the non-smooth boundary, stable curves EB_1^+, EB_3^+, $LC2^+$, $LC3^+$ and unstable curves EB_2^+, EB_6^+ are not realizable.

When the amplitude A of w is changed, the equilibrium bifurcation diagram is different (see Fig.3). Moreover, the degree of oscillation is also affected. Thus, new bursting phenomena may appear in these two cases: case A: $A = 3$, case B: $A = 7$. The mechanism will be discussed with the corresponding graphs below. In system (1), we set $a = 0.8$, $b = 0.4$, $n = 2$, and $k = 0.6$.

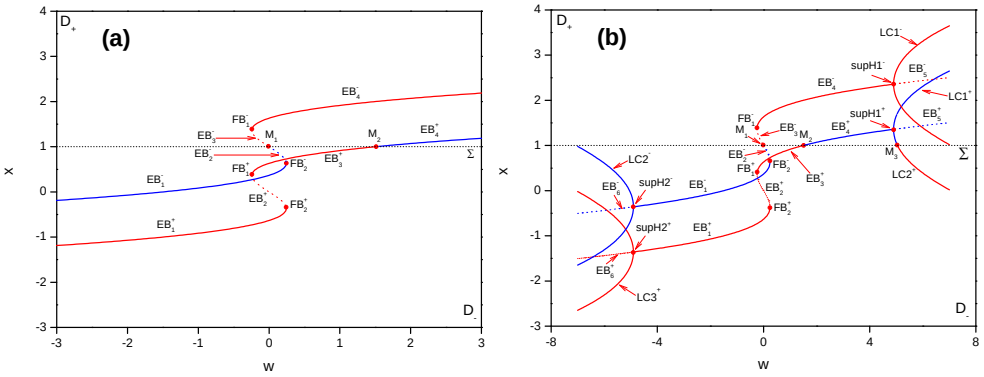

Fig. 3. The equilibrium distribution and bifurcation diagrams of the type-I system. (a) $w = [-3, 3]$, (b) $w = [-7, 7]$.

4.1.1 Asymmetric Fold/Fold bursting

In case A, we consider $A = 3$, so w changes between -3 and 3, and the system only includes four Fold bifurcation points.

Fig. 4 shows the time-domain waveforms and corresponding partial enlargement of this case. One can know that the system state variable x has continuous switching between relatively sharp oscillations and relatively slight oscillations, respectively corresponding to the SP stage and the QS stage, which manifests a typical bursting oscillations behavior. However, compared with the traditional memristor-based SM system, there is not such a feature of symmetry in the bursting oscillations because of the following three phenomena: (1) the system trajectory passes through the non-smooth boundary many times (see Fig. 4(b), Fig. 5(a)), (2) when the system trajectory arrives at the non-smooth boundary, sliding phenomena will be produced (see Fig. 4(b), Fig. 4(d)), (3) the oscillation period of the SP is different between the region D_+ and D_- (see Fig. 4(b), Fig. 4(c)).

Concerning the phenomenon (3), in Fig. 4(c), the system trajectory is always located in the region D_- which means that the oscillation frequency is only determined by the subsystem in D_-. The value of the T2 is 5.7ms. However, in Fig. 4(b), since the system trajectory passes through the boundary many times, its oscillation frequency is alternately controlled by the subsystem D_- and the subsystem D_+, in other words, the frequency is determined by both of them. The value of T1 is 1.3ms.

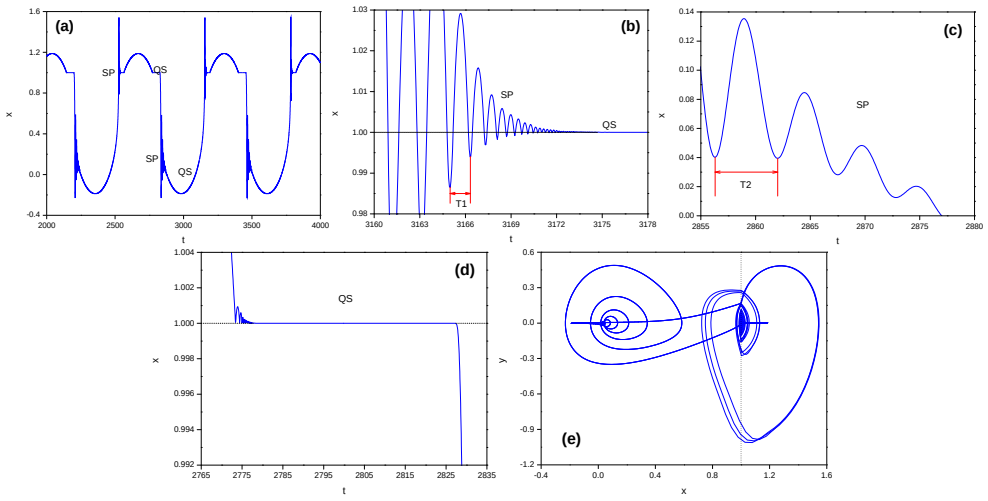

Fig. 4. Asymmetric Fold-Fold bursting oscillators for $A = 3$: (a) time-domain waveform of x, (b), (c), (d) local enlargement figurations of (a), (e) phase portrait on $x - y$ plane.

The transformed phase portrait with the overlapped equilibrium point curves (see Fig.5(b)) can help us observe the process of bursting oscillations more clearly. Supposing M_4 is the start point which is in the region D_-, so the trajectory is controlled by the subsystem D_-. It almost moves along EB_1^- and stays QS. When the trajectory arrives at FB_2^-, the equilibrium point becomes unstable and the jump phenomenon occurs. At this point, the system trajectory is still in the region D_-, controlled by the subsystem D_-, so the trajectory should theoretically jump from D_- to the equilibrium curve EB_4^- in D_+.

However, in the process of jumping, once the system trajectory passes across the non-smooth boundary into D_+, the subsystem which controls the trajectory is replaced by the subsystem D_+. For the stable equilibrium curve of the subsystem D_+ is in D_-, the trajectory passes through the boundary back into D_- and has again been controlled by the subsystem D_-. Likewise, because of the control of the subsystem D_-, the trajectory will jump to the equilibrium curve EB_4^- in D_+ again. Thus, when the stable equilibrium curve and the corresponding subsystem are located in different regions, the subsystem which controls the trajectory will change back and forth, causing the system trajectory crosses the boundary frequently and implying the transition from QS to SP. In case A, since the amplitude of w is small, the oscillations will decrease rapidly. The distance between the boundary and the trajectory reduces to zero when the trajectory has not achieved M_2, the system turns to QS. At the moment, the trajectory is still under the control of the two subsystems, so it can only move along the boundary, namely, the special damped oscillation-sliding. When the trajectory slides to M_2, if it enters the region D_+, since the equilibrium curve EB_4^+ of the subsystem D_+ is also in D_+, the trajectory will move along EB_4^+ until it reaches M_5.

After that, the parameter w decreases gradually, the system remains QS. When the trajectory reaches the intersection point M_2 between the stable equilibrium curve EB_4^+ and the non-smooth boundary, if the trajectory passes M_2 from D_+ to D_-, it will be controlled by the subsystem D_-. However, the stable equilibrium curve EB_4^- of the corresponding subsystem is in D_+, so the trajectory will return to D_+ and be controlled by the subsystem D_+. Similarly, the stable equilibrium curve EB_3^+ of the subsystem D_+ is located in D_-, therefore, the trajectory will move back to D_-

again. From the previous analysis, the stable equilibrium curve and the corresponding subsystem are located in different regions, what is more, the distance between M_2 and the boundary is zero, so the trajectory forms a sliding phenomenon.

When the system trajectory slides to the point M_1, if the trajectory enters D_-, since the stable equilibrium curve EB_1^- of the subsystem D_- is also in D_-, the trajectory will jump to EB_1^- and it will gradually approach EB_1^- during the jump. The system converts back to SP. With the further decrease of w, the trajectory finally stabilizes at EB_1^-, forming the stage of QS. When the trajectory moves to the start point M_4, a full period of the oscillatory motion ends.

In this case, on the one hand, the bursting oscillations are related to Fold bifurcation. On the other hand, when w increases and decreases, the bursting oscillations are not symmetric due to the switching control of different subsystems. Thus, the bursting pattern can be classified as asymmetric Fold/Fold busting.

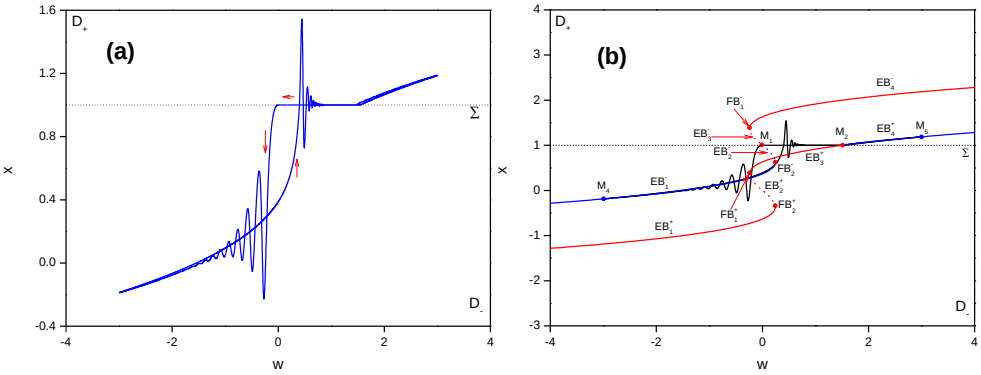

Fig. 5. Asymmetric Fold-Fold bursting oscillators for $A = 3$: (a) transformed phase portrait on $w-x$ plane, (b) transformed phase portrait with the overlapped equilibrium point curves.

4.1.2 Asymmetric Fold/Fold-delayed supHopf/supHopf bursting

Setting $A = 7$, the system includes four Fold bifurcation points and four Hopf bifurcation points. Therefore, more special oscillations may occur. Comparing Fig. 6(a), (b) with Fig. 4(a), (e), it is true that the bursting phenomena are different.

Similarly, we will use the transformed phase portrait overlapped with the equilibrium distribution curves (see Fig. 6(d)) to demonstrate the bursting oscillation and bifurcation mechanism in this case. Assuming that the curve starts from M_4, because of the Hopf bifurcation, the system firstly manifests itself as SP and forms sharp oscillations within the stable limit cycle $LC2^-$. When the trajectory moves to $supH2^-$, $LC2^-$ disappears, the stable equilibrium curve EB_1^- takes place. In theory, the system will change from SP to QS, however, due to the delay effect, periodic oscillations will continue for a while. Then the oscillation of the system decreases, resulting in QS. The trajectory will stabilize at EB_1^- and move along it. As w increases to 0.24, the equilibrium point becomes unstable, causing the trajectory jumps.

As same as case A, during the jump, the trajectory passes across the boundary. The subsystem which controls the trajectory will change back and forth since the stable equilibrium curve and the corresponding subsystem are located in different regions. The system trajectory crosses the boundary many times, implying the transition from QS to SP. However, unlike case A, since the amplitude of excitation w is much bigger, the oscillation will decrease more slowly. The distance between the trajectory

and the non-smooth boundary is not zero until it moves to M_2. As a result, the sliding phenomenon does not appear.

When the trajectory moves to M_2, if it enters the region D_+, for the stable equilibrium curve EB_4^+ of the subsystem D_+ is also located in D_+, the trajectory will move along EB_4^+, changing from SP to QS. Hopf bifurcation occurs and limit cycles are observed when $w = 4.9$, however, until w increases to 7, the system is almost in QS, the reason is also the delay effect of the supHopf bifurcation point.

When w reduces, the trajectory moves from M_5, due to the Hopf bifurcation, the system is in SP and sharp oscillations occur. However, different from the former, the stable limit cycles are not all in the region D_+. Once the trajectory moves from D_+ to D_- across the non-smooth boundary, the system is controlled by the subsystem D_-. Since the stable limit cycle $LC1^-$ of the corresponding subsystem is in D_+, the trajectory will move back to D_+ and be attracted by the subsystem D_+ once again. Likewise, there is a stable limit cycle $LC2^+$ of the subsystem D_+ in D_-, so the trajectory will return to D_- soon. Based on the above, when w decreases from M_5 to $supH1^+$, since the controlling subsystem and the corresponding stable limit cycles are located in different regions, once the trajectory moves across the boundary to another region, there is a trend of return. Under the effect of alternating control between the two subsystems, the extent of the Hopf bifurcation will be compressed, namely, the compressed oscillation phenomenon within the limit cycle.

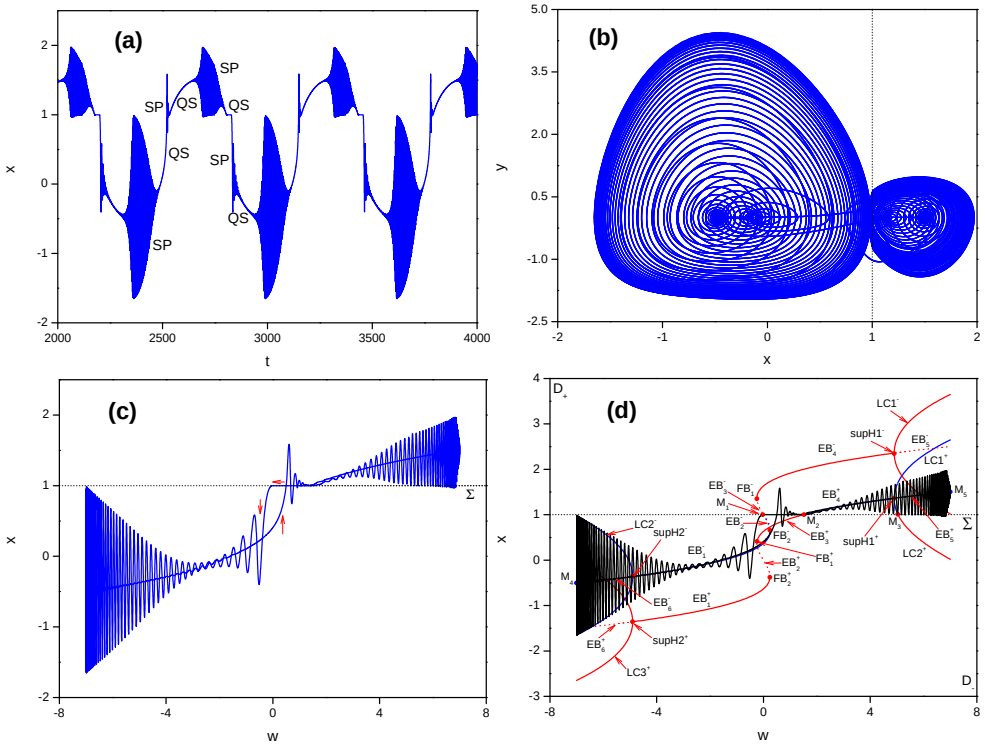

Fig. 6. Asymmetric Fold/Fold-delayed supHopf/supHopf for $A = 7$: (a) time-domain waveform of x, (b) phase portrait on $x - y$ plane, (c) transformed phase portrait on $w - x$ plane, (d) transformed phase portrait on $w - x$ plane with overlapped equilibrium point curves.

As the trajectory moves to $supH1^+$, the stable limit cycles disappear. Likewise, due to the delay effect, the trajectory does not immediately move along EB_4^+ but continues to oscillate for some time before changing from SP to QS. Consistent with case A, when the trajectory moves to M_2, it will slide to M_1 since the stable equilibrium curve and the corresponding subsystem are located in different regions. If the trajectory enters D_-, because the stable equilibrium curve EB_1^- of the subsystem D_- is also in D_-, the trajectory will jump down to EB_1^-, entering the SP stage. During the jump, the curve gradually approaches EB_1^- and finally stabilizes at it, forming QS. When the curve reaches $supH2^-$, influenced by Hopf bifurcation, the stable limit cycle $LC2^-$ occurs. The system should enter SP, however, QS will last for a while until the trajectory enters SP because of the delay effect. When w decreases to -7, a cycle of motion completes.

From the analyses above, affected by the Fold bifurcation points and Hopf bifurcation points, bursting oscillations occur four times in a cycle (see Fig. 6(a)). However, due to the existence of the non-smooth boundary, the bursting oscillations are not symmetric, like the sliding phenomenon and the compressed oscillation phenomenon. Case B can be named as asymmetric Fold/Fold-delayed supHopf/supHopf bursting.

4.2 Type-II piecewise-smooth memristor-based SM system

Similar to 4.1, 3 subsystems (see Fig. 2) are merged into a whole system and the bifurcation sets of w are illustrated in Fig. 7. The solid lines manifest stable solutions and the unstable solutions are presented by dotted lines. Although the red curves indicate the solutions exist, because of the non-smooth boundary, such solutions cannot be achieved. On the contrary, the curves shown in blue are real because the solutions and the corresponding subsystem are in the same domain. It is easy to find the blue curves in Fig. 7 correspond to the curves in Fig. 2.

As shown in Fig. 7, each of these three subsystems contains two Fold bifurcation points and two Hopf bifurcation points. There are two intersection points, respectively, M_2(1.51,2), which is between the equilibrium curve of the subsystem D_α and the non-smooth boundary Σ_1; M_1(-1.51,-2), which is between the equilibrium curve of the subsystem D_γ and the non-smooth boundary Σ_2. Fold bifurcation points are FB_1^α(-0.24,1.37) and FB_2^α(0.24,0.63) for the subsystem D_α, FB_1^β(-0.24,0.37) and FB_2^β(0.24,-0.37) for the subsystem D_β, FB_1^γ(-0.24,-0.63) and FB_2^γ(0.24,-1.37) for the subsystem D_γ; Hopf bifurcation points are $supH1^\alpha$(4.90,2.36) and $supH2^\alpha$(-4.90,-0.36) for the subsystem D_α, $supH1^\beta$(4.90,1.36) and $supH2^\beta$(-4.90,-1.36) for the subsystem D_β, $supH1^\gamma$(4.90,0.36) and $supH2^\gamma$(-4.90,-2.36) for the subsystem D_γ. The equilibrium curves and limit cycles are divided into 27 sections due to the influence of the bifurcation points and the non-smooth boundaries. Take the subsystem D_α as an example, its equilibrium curve and limit cycles are divided into six parts and three parts, respectively. Wherein, EB_1^α and $LC1^\alpha$ are stable and can be achieved; EB_2^α, EB_4^α, $LC2^\alpha$, and $LC3^\alpha$ are stable, however, due to the influence of the non-smooth boundary Σ_1, they cannot be achieved. EB_3^α is unstable and not realizable because of Fold bifurcations and the boundary Σ_1. EB_5^α and EB_6^α are unstable due to Hopf bifurcations, and only the former is realizable because of Σ_1. The segmentation analyses of equilibrium curves and limit cycles in the subsystem D_β and the subsystem D_γ are similar to those of the subsystem D_α.

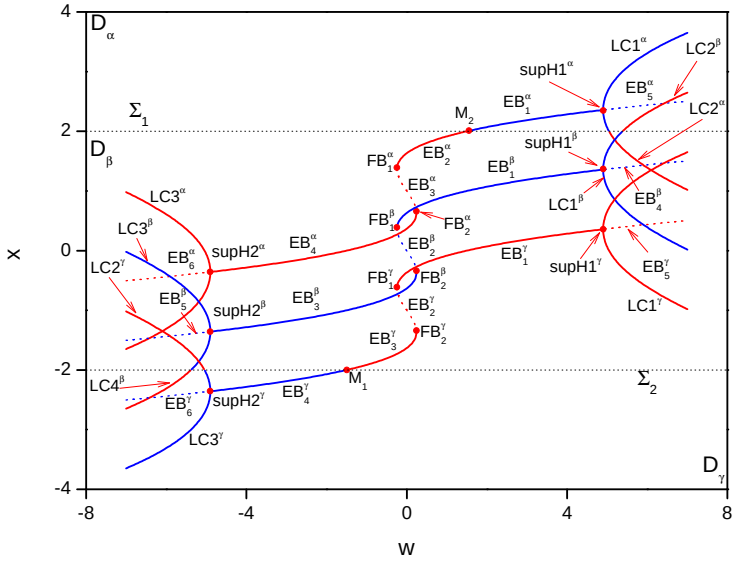

Fig. 7. The equilibrium distribution and bifurcation diagram for the type-II system.

4.2.1 Random bursting

From the previous discussion, one can find that the equilibrium distribution and bifurcation diagram of the type-II system is more complex due to the change of the piecewise function. The type-II system will be discussed under the assumption that the amplitude of the excitation w is 7.

Compared with the type-I system, Fig. 8(a) manifests the biggest difference is that the bursting phenomenon is no longer cyclical. In each period of w, whether w increases from -7 to 7 or decreases from 7 to -7, the number of bursting oscillations is three or four, randomly. For convenience, there are four types of bursting oscillations, namely, A, B, C, and D (see Fig. 9). As w increases from -7 to 7, type-A means the bursting phenomenon occurs three times, type-B means the number of bursting oscillations is four; When w decreases from 7 to -7, type-C corresponds to type-A, type-D corresponds to type-B. So, during the period of w, A, B and C, D will be combined freely, with random combinations of A-C, A-D, B-C, and B-D.

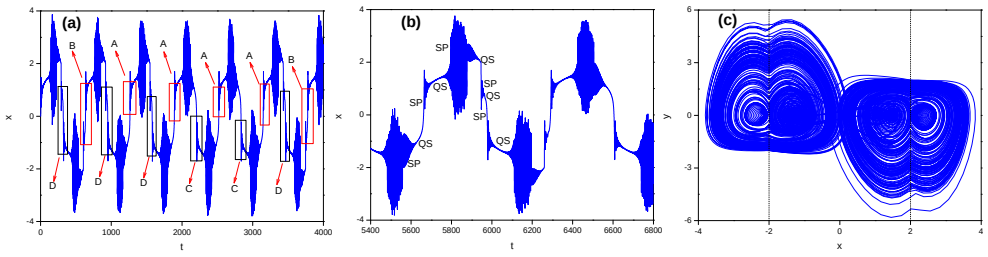

Fig. 8. Random bursting oscillations for $A = 7$: (a) time-domain waveform of x, (b) local enlargement figuration of time-domain waveform of x, (c) phase portrait on $x - y$ plane.

To analyze the process of bursting oscillations, the transformed phase portraits on $w-x$ plane and the corresponding overlapped diagrams with equilibrium point curves are shown in Fig. 9.

Firstly, when w increases from -7 to 7, as for the type-A bursting phenomenon (see Fig. 9(a) and (b)), assuming that the oscillations start at M_3, the trajectory is controlled by the subsystem D_β. Due to the influence of the stable limit cycles $LC3^\beta$ and $LC4^\beta$, the system manifests itself as SP and the trajectory begins to sharply oscillate. Since $LC4^\beta$ is in D_γ, once the system trajectory enters D_γ, it will be attracted by the corresponding subsystem, in other words, $LC2^\gamma$ and $LC3^\gamma$. As we can see, only $LC3^\beta$, $LC3^\gamma$ and their corresponding subsystems are in the same region. Thus, in the initial stage, the trajectory oscillates within $LC3^\beta$ and $LC3^\gamma$, namely, double loop oscillations. Since the control abilities of the subsystem D_β and the subsystem D_γ are almost identical, with the further increase of w, the system trajectory may eventually be captured by $LC2^\gamma$ and $LC3^\gamma$ or $LC3^\beta$ and $LC4^\beta$. As for type-A, the trajectory is captured by the latter and continues to oscillate in the region D_β. When w increases to -4.9, limit cycles disappear, however, due to the delay effect, the periodic oscillations continue for a while before the trajectory moves along the stable equilibrium curve EB_3^β, changing from SP to QS. The equilibrium point loses its stability when the trajectory arrives at FB_2^β. Soon jump phenomenon happens, implying the transition from QS to SP, bursting oscillations occur.

As w continues to increase, the amplitude of oscillations decays gradually and then the system trajectory moves along EB_1^β, entering the QS stage. When the trajectory reaches $supH1^\beta$, limit cycles occur, however, because of the delay effect, the system will keep QS over a period of time. After that, the trajectory oscillates sharply due to Hopf bifurcation and the system enters the SP stage.

For the type-B bursting phenomenon (see Fig. 9(c), (d)), which corresponds to the situation that the trajectory is finally captured by the limit cycle $LC2^\gamma$ and $LC3^\gamma$, the trajectory oscillates in D_γ. When w increases to -4.9, the limit cycles disappear, due to the delay effect, the trajectory continues to oscillate for some time before it moves along EB_4^γ and enters the QS stage. As the trajectory moves to M_1, because of the non-smooth boundary Σ_2, the trajectory will jump to the stable equilibrium curve EB_3^β, triggering a bursting phenomenon. After that, w continues to increase, the amplitude of oscillations rapidly decreases and the trajectory moves along the stable equilibrium curve EB_3^β, leading to the change from SP to QS.

When the trajectory reaches FB_2^β, due to the influence of Fold bifurcations, the equilibrium point becomes unstable again, which leads to the jump to EB_1^β. The bursting oscillations occur again, implying the transition from QS to SP. Then, as w increases further, the amplitude of the system reduces and the trajectory moves along EB_1^β, entering the QS stage. When w increases to 4.9, the limit cycles appear, however, the QS stage will keep for a while due to the delay effect. After that, the system enters the SP stage and the trajectory oscillates sharply.

Similarly, when w decreases from 7 to -7, type-C (see Fig. 9(e), (f)) and type-D (see Fig. 9(g), (h)) bursting phenomena may occur, corresponding to type-A and type-B, respectively. The details of the analyses will not be presented here.

To sum up, the randomness of the bursting oscillations in the type-II system is decided by the special structure of the equilibrium distribution and bifurcation. Within the limit cycles, during the sharp oscillations, the two subsystems will compete for the control of the trajectory, which leads to the uncertain skewing of the trajectory. So, the bursting pattern can be called random bursting.

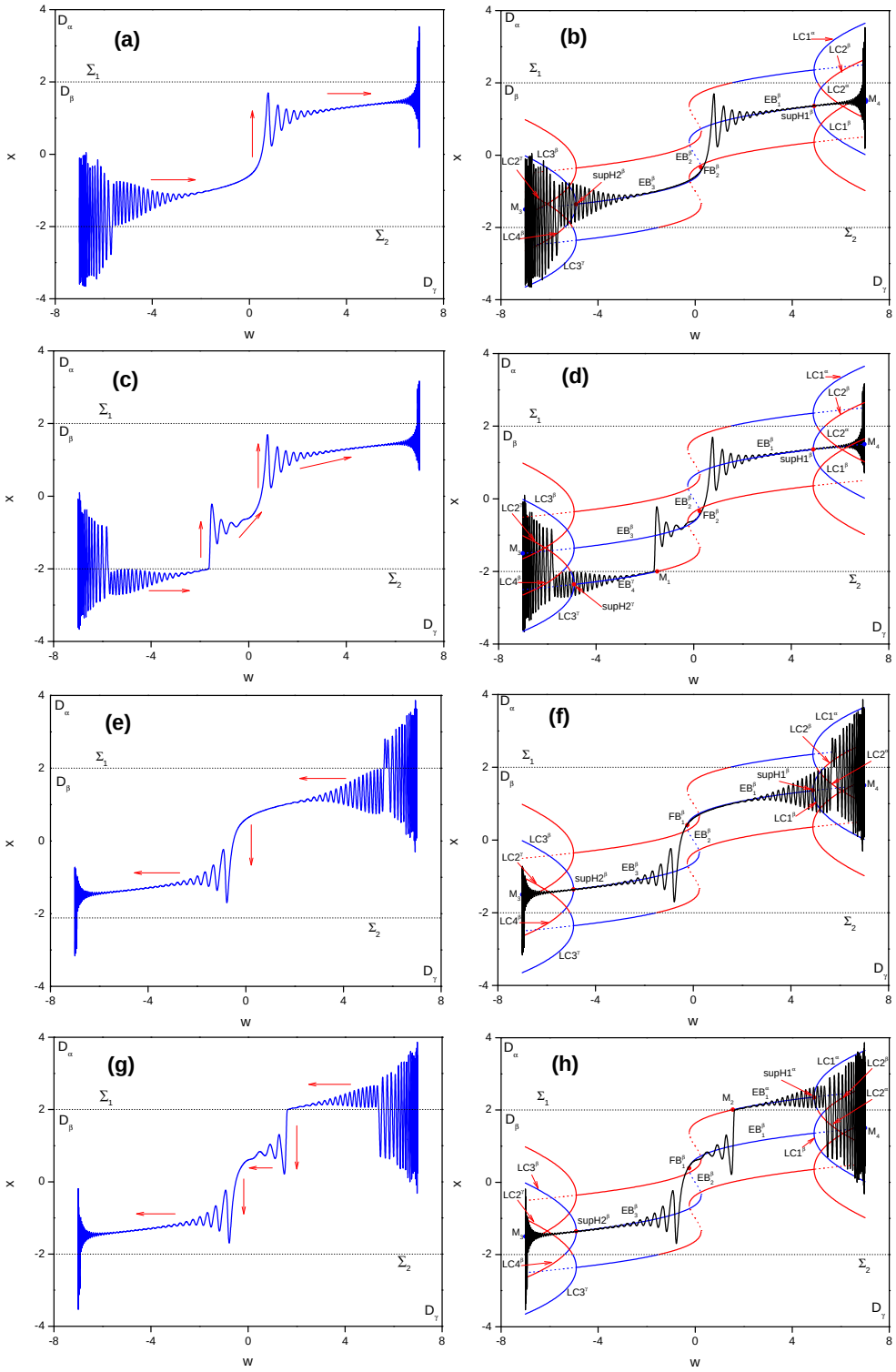

Fig. 9. Random bursting for $A = 7$: transformed phase portrait on $w - x$ plane and transformed phase portrait on $w - x$ plane with overlapped equilibrium point curves, (a), (b) type-A bursting, (c), (d) type-B bursting, (e), (f) type-C bursting, (g), (h) type-D bursting.

5 Circuit simulation

A simulation circuit of system (1) in Cadence is built to verify the authenticity of the bursting phenomena discussed above. To achieve low voltage, the circuit is scaled. The schematic of this circuit is shown in Fig. 10. V_2 and V_3 are DC power supplies of 0.5V and 1V, respectively. It should be noted that the low voltage low power operational amplifier (OA) for the fully integrated piecewise-smooth chaotic system is presented in Fig. 11 [36]. The supply voltage of this operational amplifier is $V_{CC} = -V_{SS} = 2.5$V. The designed OA is made up of three parts, the bias circuit, the differential input circuit, and the output circuit.

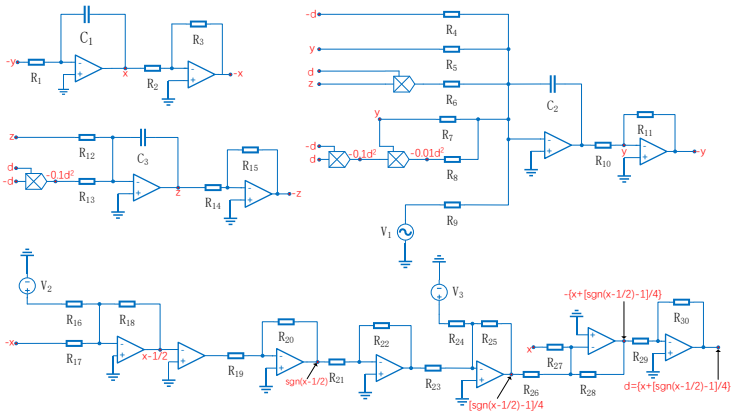

Fig. 10. Cadence simulation circuit of the type-I piecewise-smooth memristor-based SM system.

By using Cadence IC Design Tools with the chart18 CMOS process, we can analyze the amplitude and phase frequency characteristics of the OA (see Fig. 12). Its voltage gain is 54.73dB and the phase margin is 85.96°. Its power consumption is about 1.2mW with ±2.5V supply voltage.

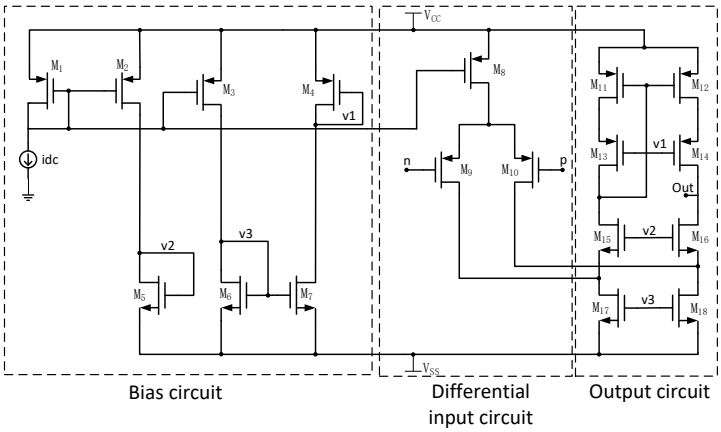

Fig. 11. The designed operational amplifier.

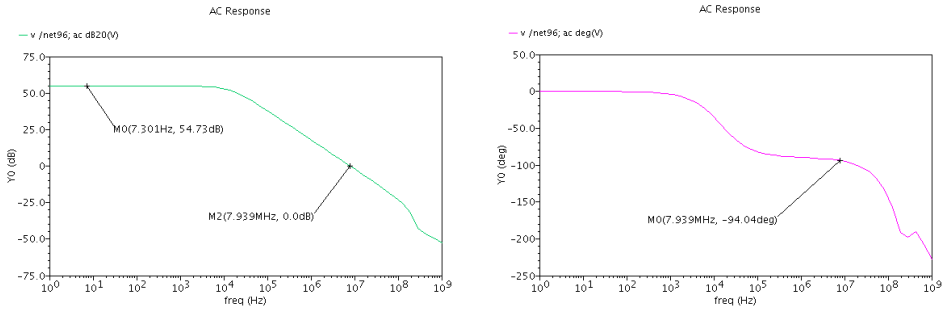

Fig. 12. The amplitude and phase fequency characteristics of the operational amplifier.

As for the multiplier in Fig. 10, a low voltage low power CMOS four-quadrant analog multiplier is presented in Fig. 13 [37]. To verify the function of this multiplier, two sinusoidal voltages were input to the circuit, where V_{Yd} was a 5-MHz carrier signal with peak amplitude of 0.4V and V_{Xd} was a 200-kHz modulating signal with the same amplitude. We can obtain the double sideband AM signal waveform in Fig. 13. Moreover, this multiplier consumes about 3.9mW of quiescent power.

To sum up, the power consumption of the whole circuit is about 31.2mW with ±2.5V supply voltage.

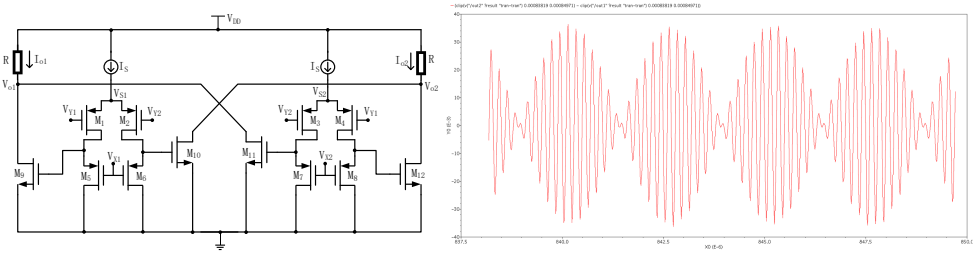

Fig. 13. Proposed multiplier circuit and the corresponding transient response.

According to Kirchhoff's laws, the circuit in Fig.10 can be listed as follows

$$\begin{aligned}
\frac{dv_x}{dt} &= \frac{1}{R_1C_1}y \\
\frac{dv_y}{dt} &= \frac{1}{R_4C_2}[x+g(x)] - \frac{1}{R_5C_2}y - \frac{0.1}{R_6C_2}z[x+g(x)] + \frac{1}{R_9C_2}V_1 \\
&+ \{\frac{0.01}{R_8C_2}[x+g(x)]^2 - \frac{1}{R_7C_2}\}y \\
\frac{dv_z}{dt} &= \frac{0.1}{R_{13}C_3}[x+g(x)]^2 - \frac{1}{R_{12}C_3}z
\end{aligned} \tag{10}$$

Wherein, we set the output voltages of the OA as V_x, V_y, and V_z, respectively. The slow-varying parameter corresponds to $V_1 = Asin(2\pi ft)$. Considering the proportional compression effect and analyzing the relationship between (10) and (1), one can figure out the value of circuit elements, which are illustrated in Table 1. What calls for special attention is that capacitors over 40 pF do not apply to integrated circuits based on the chart18 CMOS process. Thus, ten 25 pF capacitors are paralleled to realize one 250 pF capacitor in the practical circuit.

The amplitude of the excitation V_1 is set as $A = 1.5$V with the excitation frequency $f = 1.59$Hz. According to the related time-domain waveform of x and the phase portrait in Fig. 14, the circuit manifests asymmetric Fold/Fold bursting. Compared Fig. 14 with Fig. 4, the Cadence simulation results and the MATLAB simulation results are consistent. It is a piece of convictive evidence that such complex bursting oscillators surely exist in the piecewise-smooth memristor-based SM system.

Table 1. The value of circuit elements

Parameters	Significations	Values
C_1 C_2 C_3	Capacitance	250pF
R_2 R_3 R_{20}	Resistance	1kΩ
R_{25}	Resistance	2.5kΩ
R_{10} R_{11} R_{14}-R_{18} R_{21}-R_{24} R_{26}-R_{30}	Resistance	10kΩ
R_{19}	Resistance	13.5kΩ
R_8	Resistance	16.7kΩ
R_6 R_{13}	Resistance	200kΩ
R_7	Resistance	3.33MΩ
R_1 R_4 R_9	Resistance	4MΩ
R_5	Resistance	5MΩ
R_{12}	Resistance	10MΩ

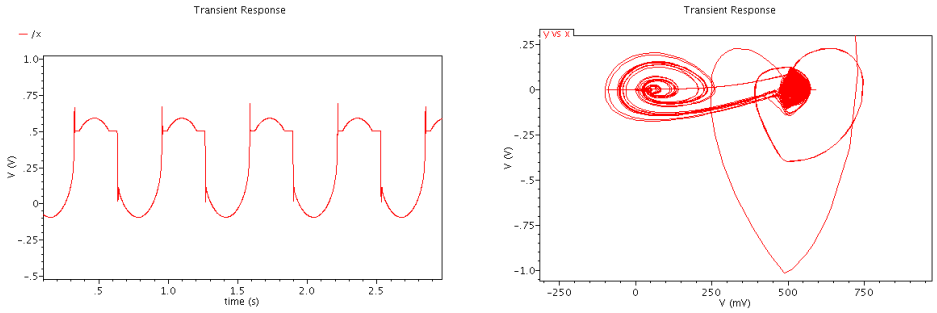

Fig. 14. Simulation results of the type-I piecewise-smooth memristor-based SM system for $A = 3$. (a) time-domain waveform of x, (b) phase portrait on $x - y$ plane.

6 Conclusion

This paper discussed relevant issues on a fully integrated piecewise-smooth chaotic system. Firstly, A piecewise-smooth memristor-based SM system has been built mathematically. According to different piecewise functions, two systems are considered. Based on the amplitude of the excitation w and the type of the piecewise function, different bursting phenomena are revealed. The corresponding bifurcation mechanisms are analyzed by using the transformed phase portraits, the time-domain waveforms, and the phase portraits. It is found that not only the properties of the nominal equilibrium orbits and limit cycles but also the existence of the non-smooth boundary contributes to the sorts of bursting phenomena. For feasibility, the practical circuit is

fully integrated in Cadence. The circuit simulations are conducted to verify the correctness of these new bursting phenomena, and the results are identical to theoretical analyses. Our study broadens the area of bursting dynamics.

Acknowledgments

This work was supported in part by the National key R & D program of China under Grant 2018AAA0103300.

References

1. R. Zhang, M. Peng, Z. D. Zhang, Q. S. Bi, Chinese Physics B **27** (11), (2018) 416-22
2. Z. D. Zhang, B. B. Liu, Q. S. Bi, Nonlinear Dynamics **79** (1), (2015) 195-203
3. Q. S. Bi, X. K. Chen, J. Kurths, Z. D. Zhang, Nonlinear Dynamics **85** (4), (2016) 2233-45
4. X. H. Li, J. Y. Hou, International Journal of Non-Linear Mechanics **81**, (2016) 165-76
5. L. Wang, X. S. Yang, Nonlinear Dynamics **97** (4), (2019) 2469-81
6. D. H. Li, H. B. Chen, J. H. Xie, International Journal of Bifurcation & Chaos **29** (4), (2019) 1950051
7. N. Ramou, Russian Journal of Nondestructive Testing **55** (2), (2019) 155-61
8. R. Cristiano, D. J. Pagano, Journal of Nonlinear Science **29** (3), (2019) 2845-75
9. S. T. Kingni, L. Keuninckx, P. Woafo, G. Sande, J. Danckaert, Nonlinear Dynamics **73** (1-2), (2013) 1111-23
10. A. M. N. Kiss, B. Marx, G. Mourot, G. Schutz, J. Ragot, Control Engineering Practice **19** (11), (2011) 1354-62
11. M. Kess, C. Brüning, V. Engel, Chemical Physics **442** (11), (2014) 26-30
12. Q. S. Bi, Science China Technological Sciences **53** (2), (2010) 748-60
13. B. R. Miller, A. G. Walker, A. S. Shah, S. J. Barton, G. V. Rebec, Journal of Neurophysiology **100** (4), (2008) 2205-16
14. Z. D. Zhang, Y. Y. Li, Q. S. Bi, Physics Letters A **377** (13), (2013) 975-80
15. Izhikevich, M. Eugene, International Journal of Bifurcation and Chaos **10** (06), (2000) 1171-266
16. D. Cafagna, G. Grassi, Math Problem in Engineering **2013**, (2013) 1-7
17. V. T. Pham, A. Ouannas, C. Volos, T. Kapitaniak, AEU-International Journal of Electronics and Communications **86**, (2018) 69-76
18. G. S. Yi, J. Wang, X. L. Wei, B. Deng, H. Y. Li, C. X. Han, Applied Mathematics & Computation **231**, (2014) 100-10
19. F. Grgoire-Lacoste, V. Jacquemet, A. Vinet, Mathematical Biosciences **250**, (2014) 10-25
20. L. O. Chua, *Memristor-the missing circuit element* (IEEE Transactions, 1971) 507–19
21. Q. W. Tan, Y. C. Zeng, Z. J. Li, Nonlinear Dynamics **94** (3), (2018) 1585–602
22. Galias, Zbigniew, IEEE Transactions on Circuits & Systems II Express Briefs **65** (5), (2018) 637–41
23. J. Kengne, A. Nguomkam Negou, D. Tchiotsop, Nonlinear Dynamics **88**, (2017) 2589–608
24. C. Zhou, C. H. Wang, Y. Sun, W. Yao, Neurocomputing **403**, (2020) 225-32
25. H. Bao, N. Wang, B. C. Bao, M. Chen, P. P. Jin, G. Y. Wang, Communications in Nonlin-ear Science & Numerical Simulation **57**, (2018) 264-75
26. Q. H. Fu, J. Y. Cai, S. M. Zhong, International Journal of Control Automation and Systems **17**, (2019) 2666-76
27. X. T. Min, X. Y. Wang, P. F. Zhou, S. M. Yu, H. H. C. Iu, IEEE Access **99**, (2019) 124641-46
28. Q. Lai, Z. Q. Wan , P. D. K. Kuate, H. Fotsin, Communications in Nonlinear Science and Numerical Simulation **89**, (2020) 105341

29. N. H. Alombah, H. Fotsin, K. Romanic, International Journal of Bifurcation & Chaos in Applied Sciences & Engineering **27** (05), (2017) 1750067
30. N. Wang, G. S. Zhang, H. Bao, Nonlinear Dynamics **97**, (2019) 1477-94
31. Z. H. Wen, Z. J. Li, X. Li, Chaos, Solitons & Fractals **128**, (2019) 58-70
32. B. C. Bao, P. Wu, H. Bao, H. G. Wu, X. Zhang, M. Chen, Chaos Solitons & Fractals **109**, (2018) 146-53
33. H. G. Wu, B. C. Bao, Z. Liu, Q. Xu, P. Jiang, Nonlinear Dynamics **83**, (2015) 893–903
34. J. Jin, LV Zhao, Journal of Circuits, Systems and Computers **27** (10), (2018) 1850155
35. J. Jin, Microelectronics Journal **75**, (2018) 27-34
36. B. Razavi, *Design of Analog CMOS Integrated Circuits* (McGraw-Hill Education, 2016) 389
37. C. Sawigun, J. Mahattanakul, IEEE International Symposium on Circuits and Systems, (2008) 2318-21